Journal of Crystal Growth 474 (2017) 69–75

Contents lists available at ScienceDirect

Journal of Crystal Growth

journal homepage: www.elsevier.com/locate/jcrysgro

Numerical analysis of impurity separation from waste salt by investigating the change of concentration at the interface during zone refining process

Ho-Gil Choi[a], Moonsoo Shim[b], Jong-Hyeon Lee[b], Kyung-Woo Yi[a,*]

[a] Department of Materials Science and Engineering, Seoul National University, Seoul 151-744, South Korea
[b] Department of Materials Science and Engineering, Chungnam National University, Daejeon 305-764, South Korea

ARTICLE INFO

Communicated by Dr Francois Dupret

Keywords:
B1. Lithium chloride
A2. Zone refining
A1. 3-D simulation
A1. Decontamination factor

ABSTRACT

The waste salt treatment process is required for the reuse of purified salts, and for the disposal of the fission products contained in waste salt during pyroprocessing. As an alternative to existing fission product separation methods, the horizontal zone refining process is used in this study for the purification of waste salt. In order to evaluate the purification ability of the process, three-dimensional simulation is conducted, considering heat transfer, melt flow, and mass transfer. Impurity distributions and decontamination factors are calculated as a function of the heater traverse rate, by applying a subroutine and the equilibrium segregation coefficient derived from the effective segregation coefficients. For multipass cases, 1d solutions and the effective segregation coefficient obtained from three-dimensional simulation are used. In the present study, the topic is not dealing with crystal growth, but the numerical technique used is nearly the same since the zone refining technique was just introduced in the treatment of waste salt from nuclear power industry because of its merit of simplicity and refining ability. So this study can show a new application of single crystal growth techniques to other fields, by taking advantage of the zone refining multipass possibility. The final goal is to achieve the same high degree of decontamination in the waste salt as in zone freezing (or reverse Bridgman) method.

1. Introduction

Pyroprocessing can be used to reprocess spent nuclear fuel, and it results in reducing both its volume and its radioactivity. According to the Pyroprocess Integrated Inactive Demonstration Facility (PRIDE) at the Korea Atomic Energy Research Institute (KAERI), pyroprocessing consists of several unit processes: the head-end process (to fabricate a feed material for electrolytic reduction), the electrolytic reduction process, the electrorefining process, the electrowinning process, and the waste treatment process [1]. During the electrolytic reduction and electrorefining processes, waste salts are generated. Both the LiCl salt waste from electrolytic reduction, and the LiCl-KCl eutectic salt from electrorefining incorporate Groups I and II fission products such as Cs and Sr. Due to the high radioactivity of these fission products, they must be removed from the LiCl and LiCl-KCl eutectic waste salts to allow the reuse of these salts. Moreover, they have to be disposed of in a chemically stable waste form that is adequate for long-term geologic storage.

The conventional process for removing fission products from waste salt consists of occlusion and ion exchange by zeolites [2]. This process can remove all fission products from the waste salt, but has the problems of generating a large amount of waste, as well as limited ion absorption capacity. To replace the conventional process, various separation processes, such as the zone freezing process [3,4] and the Czochralski process [5] have been investigated. Even though these processes show effective removal of the fission products from waste salt, the proceeding rate is at a level of millimeters per hour. In the present study, the zone refining process is used as a purification process to utilize its higher proceeding rate. In addition, the zone refining process can be repeated for additional separation of fission products.

In the present study, a three-dimensional transient model is used to calculate the impurity (e.g., fission products such as Cs and Sr) concentrations at every position in the specimen. Changing the heater traverse rate, which affects the process proceeding rate, impurity concentration distributions are calculated. From the impurity concentration results, decontamination factors are obtained to calculate the degree of impurity disposal. Moreover, analytical solutions are adopted to obtain the impurity concentration distributions after each process repetition.

* Corresponding author.
E-mail address: yikw@snu.ac.kr (K.-W. Yi).

http://dx.doi.org/10.1016/j.jcrysgro.2016.12.083

Available online 23 December 2016

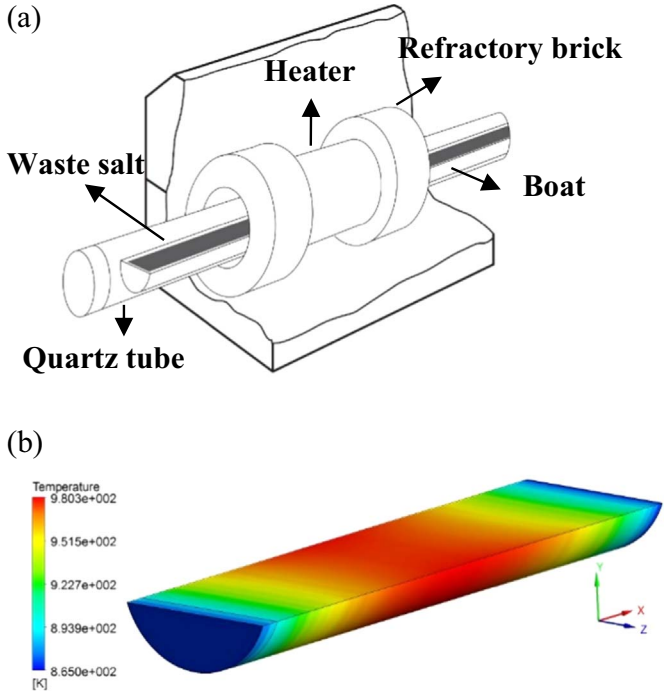

Fig. 1. (a) Schematic diagram of the zone refining equipment in case of a resistant heater and (b) separated molten zone region with thermal boundary condition.

2. Model description

2.1. Description of three-dimensional model of the zone refining process

Three-dimensional simulation is conducted to study impurity segregation during the zone refining process. The heat transfer, flow in the melt, and mass transfer are calculated by modeling the zone refining equipment of Chungnam National University (CNU), as shown in Fig. 1(a). We calculate the temperature distribution of the complete equipment. The heater used in the model is a resistant heater. We selected the heater temperature which makes the temperature distribution matching that of the equipment. In the global model, we solved heat transfer with radiation and fluid flow in the gas state and heat conduction in the salt. From the result, the length of the molten zone is about 100 mm when the heater temperature is 1000 K, and we separate the molten zone region from the rest of the equipment geometry (Fig. 1(b)). This molten zone region is used to calculate the transfer and concentration of the impurity. To consider external conditions, the temperature distribution of a specimen is used as boundary condition.

The molten zone region moves, following the heater movement. When X is the position of the freezing interface, f is the heater traverse rate, and N is the time the heater has been moving, X is equal to the product of f and N. By using this concept, the position of the freezing interface can be replaced with the process time. Meanwhile, the impurity concentration of the recrystallized solid (C_S) at the freezing interface is equal to the product of the impurity concentration of the melt at the freezing interface (C_O) and the equilibrium segregation coefficient (K_{eq}). By investigating the change in C_O through time, and applying the above concept, we can calculate C_S at every position of the specimen. Furthermore, we can obtain the impurity concentration distribution after the process by plotting C_S along the process direction.

The major assumptions of the model are as follows. The equilibrium segregation coefficient K_{eq} is a constant. The heater traverse rate and zone length are constant. The diffusion of impurities in the solid and the difference in density from the impurity concentration are negligible. The interface moving rate is equal to the heater traverse rate. The impurity concentration distribution in the specimen from one end to the other is calculated with these assumptions.

The change in impurity concentration in the melt through time is calculated with the molten zone region and the solid-liquid interfaces fixed, although the interfaces move as the heater moves. Instead of the interfaces moving, constant flow, whose value is equal to the interface moving speed with the opposite direction, is added to the melt. This flow allows the interface movement to be considered with fixed interfaces. This concept is applied to the model by means of a subroutine and wall velocity, as shown in Fig. 2(a). Details of the model are illustrated in Fig. 2(b). The recrystallizing and melting mass rates (kg/s) at each solid-liquid interface are expressed as the products of density (kg/m^3), interface area (m^2), and interface moving rate (m/s). The effect of latent heat is ignored. Whereas strong solid-liquid interface concavity can be expected due to the high growth velocities, the authors decided to simplify solid-liquid interface as plane. This assumption is simple. However, the authors think that it does not largely deteriorate the main purpose of the present study, viz. the analysis and increase of the decontamination factor. At the melting interface, the impurity mass rate mixed in the melt is expressed as the product of the initial impurity concentration of the specimen and the total mass rate. On the other hand, at the freezing interface, the escaping impurity rate from the melt is expressed as the product of the equilibrium segregation coefficient, the impurity concentration at the interface, and the total mass rate. The resulted temperature distribution and vectors of the flow in the melt is shown in Fig. 2(c), and flow streamlines by thermal boundary condition and subroutine in Fig. 2(d).

2.2. Equilibrium segregation coefficient

In the present study, the solvent is LiCl, and $SrCl_2$ is used as an impurity. The equilibrium segregation coefficient of $SrCl_2$ in LiCl is required to calculate the impurity concentration distributions. However, there is little information about the equilibrium coefficient in the literature or in thermodynamic databases. Hence, we derive the equilibrium segregation coefficient by utilizing the effective segregation coefficient from the research conducted by Y. Z. Cho et al. [4].

To obtain the equilibrium segregation coefficient, the following equations for the effective segregation coefficient expressed in terms of the equilibrium segregation coefficient are used [6–8]:

$$K_{eff}=\frac{K_{eq}}{K_{eq}+(1-K_{eq})exp\left(-\frac{f\delta}{D}\right)}, \tag{1}$$

$$K_{eff}=\frac{K_{eq}}{1-(1-K_{eq})\Delta}, \quad \Delta=\frac{f\delta}{D} or \frac{f}{h}, \tag{2}$$

where K_{eff} denotes the effective segregation coefficient, K_{eq} is the equilibrium segregation coefficient, f is the heater traverse rate, δ is the diffusion boundary layer thickness, D is the diffusion coefficient, and h is the convection mass-transfer coefficient. Eqs. (1)–(2) put into logarithm form are given as follows:

$$ln\left(\frac{1}{K_{eff}}-1\right)=-\frac{\delta}{D}f+ln\left(\frac{1}{K_{eq}}-1\right), \tag{3}$$

$$\frac{1}{K_{eff}}=\left(1-\frac{1}{K_{eq}}\right)\frac{\delta}{D}f+\frac{1}{K_{eq}} or \left(1-\frac{1}{K_{eq}}\right)\frac{1}{h}f+\frac{1}{K_{eq}}. \tag{4}$$

Consequently, one can obtain the equilibrium segregation coefficient by plotting $\ln(1/K_{eff}-1)$ [9] or $1/K_{eff}$, depending on the heater traverse rate.

2.3. Multipass distribution

The impurity concentration distribution, as a function of the

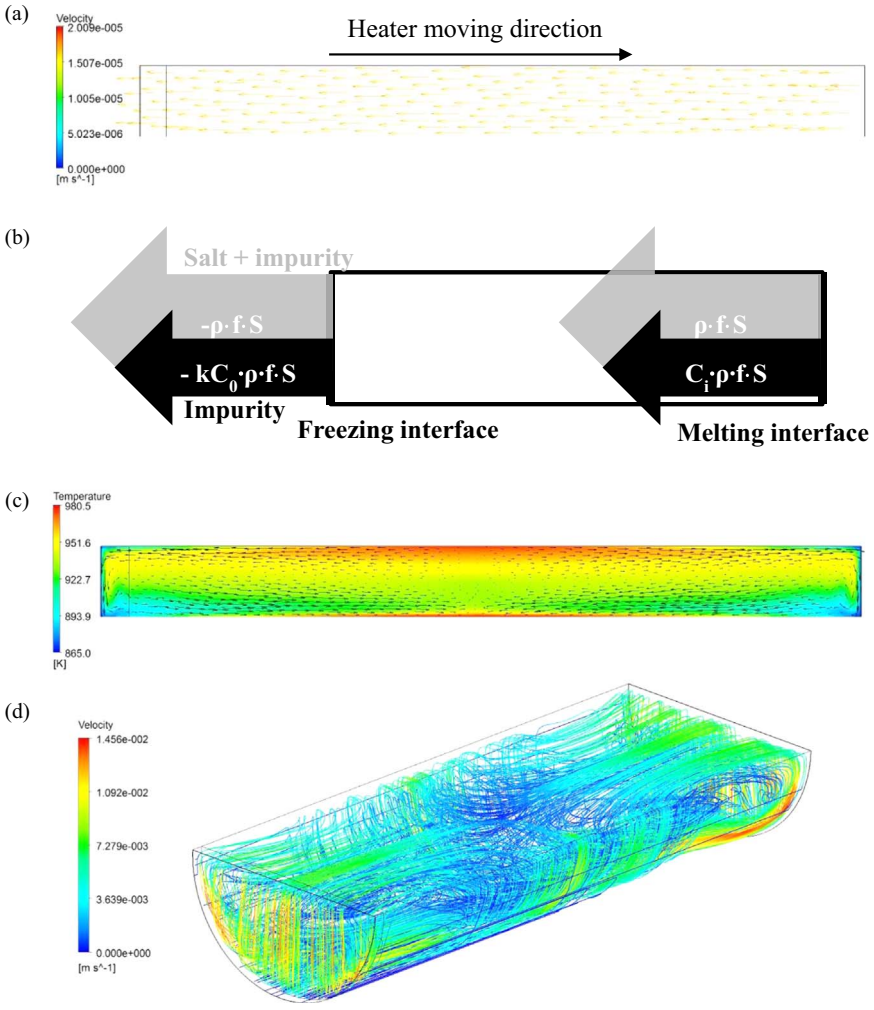

Fig. 2. (a) Generated flow by wall velocity and the subroutine (f=1 mm/min), (b) Model applied to 3D simulation, (c) the temperature distribution and flow vectors, and (d) streamlines in the melt zone.

number of passes, is calculated by means of 1D explicit solutions as suggested in the research by J. A. Spim et al. [10]. These solutions consist of four parts: X=0, $0 < X < (1\text{-}Z)$, $(1\text{-}Z) \le X < 1$, and X=1, where X denotes the normalized distance from the specimen left extremity to the solid-liquid interface along the process direction, and Z signifies the relative zone length to the specimen length at the beginning of each pass, so that $Z < 1$ since the initial zone length is lower than the specimen length. Then δX denotes a small element of relative length, and $C_{S_X}^n$ and $C_{L_X}^n$ are the unknown impurity concentration in the solid and the liquid, in the discrete segment δX located at the right of the interface of position X. The impurity concentration in the specimen is obtained as follows:

1) At the beginning of a pass, X=0, the molten zone region is placed at the left extremity of the specimen. Therefore, we have

$$C_{S_0}^n = K_{eff}\left(\sum_{i=0}^{\frac{Z-\delta X}{\delta X}} C_{S_{i\delta X}}^{n-1}\right)\left(\frac{\delta X}{Z}\right). \tag{5}$$

Indeed, from the definition of the effective segregation coefficient, we have

$$C_{S_X}^n = K_{eff}\, C_{L_X}^n. \tag{6}$$

2) For the region where the molten zone length is constant and equal to Z, $0 < X < (1\text{-}Z)$, the sum of the impurities from 0 to $X+Z$ in the specimen at $n-1$ passes is equal to the sum of the impurities from 0 to X in the specimen at the n^{th} pass, plus those in the melt, which is expressed by the following equation:

$$\left(\sum_{i=0}^{\frac{X+Z-\delta X}{\delta X}} C_{S_{i\delta X}}^{n-1}\right)\delta X = \left(\sum_{i=0}^{\frac{X-\delta X}{\delta X}} C_{S_{i\delta X}}^{n}\right)\delta X + (C_{L_X}^n)Z. \tag{7}$$

Consequently, $C_{S_X}^n$ is given by the following equation:

$$C_{S_X}^n = K_{eff}\left(\sum_{i=0}^{\frac{X+Z-\delta X}{\delta X}} C_{S_{i\delta X}}^{n-1} - \sum_{i=0}^{\frac{X-\delta X}{\delta X}} C_{S_{i\delta X}}^{n}\right)\left(\frac{\delta X}{Z}\right). \tag{8}$$

3) For the region where the molten zone length decreases with time, $(1\text{-}Z) \le X < 1$, the sum of the impurities through the entire specimen is equal to the sum of the impurities from 0 to X in the specimen at the n^{th} pass, plus those in the melt, which is expressed by the following equation:

$$C_0 = \left(\sum_{i=0}^{\frac{X-\delta X}{\delta X}} C_{S_{i\delta X}}^{n}\right)\delta X + (C_{L_X}^n)(1 - X). \tag{9}$$

Indeed, unlike the region $0 < X < (1\text{-}Z)$, the molten zone length changes along with the change in X, and is equal to $1\text{-}X$. Consequently, $C_{S_X}^n$ is given by the following equation:

$$C_{S_X}^n = K_{eff}\left(\frac{C_0}{1-X} - \left(\sum_{i=0}^{\frac{X-\delta X}{\delta X}} C_{S_{i\delta X}}^n\right)\left(\frac{\delta X}{1-X}\right)\right). \quad (10)$$

4) In general, the following equation may be applied because the total impurities in the specimen are conserved:

$$\sum_{i=0}^{\frac{1-\delta X}{\delta X}} C_{S_{i\delta X}}^{n-1} = \sum_{i=0}^{\frac{1-\delta X}{\delta X}} C_{S_{i\delta X}}^{n} = \frac{C_0}{\delta X}. \quad (11)$$

However, since an explicit scheme is used, no equation is applied at the specimen right extremity, X=1, at the right of which there is no discrete interval δX.

3. Results and discussion

3.1. Determination of the equilibrium segregation coefficient of $SrCl_2$ in LiCl

The equilibrium segregation coefficient of $SrCl_2$ in LiCl is derived from the effective segregation coefficient, which depends on the heater traverse rate, and was obtained by Y. Z. Cho et al. [4]. The method for deriving the equilibrium value is as follows. First, the values of $\ln(1/K_{eff}-1)$ are calculated as functions of the heater traverse rate, and then plotted. Additionally, a linear fitting line is obtained from the plotted points. As shown in Eq. (3), the heater traverse rate and $\ln(1/K_{eff}-1)$ have linear relationship, and the y-intercept corresponds to $\ln(1/K_{eq}-1)$, independently of the diffusion boundary layer thickness δ. Although the slope of the linear fit includes the boundary layer thickness, only the y-intercept is required to obtain the equilibrium segregation coefficient [ref.9]. Therefore, the equilibrium segregation coefficient can be obtained by calculating the y-intercept of the linear fitting line. Fig. 3(a) is the plotted result from using Eq. (3). The y-intercept of the linear fitting line has a value of 4.6860, an R-squared of 0.9556, and an equilibrium segregation coefficient of 0.0091. In addition, the calculation of the equilibrium segregation coefficient using another equation for the effective segregation coefficient, such as Eq. (4), has been conducted. As shown in Eq. (4), the heater traverse rate and $1/K_{eff}$ have linear relationship, and the y-intercept corresponds to $1/K_{eq}$, again independently of the diffusion boundary layer thickness. Therefore, the equilibrium segregation coefficient can be obtained by calculating the y-intercept of the linear fitting line. Fig. 3(b) is the plotted result using Eq. (4). The-y intercept of the linear fitting line has a value of 95.1560, an R-squared value of 0.8885, and an equilibrium segregation coefficient of 0.0105. In the present study, we use a value of 0.01 for the equilibrium segregation coefficient of $SrCl_2$ in LiCl.

3.2. Impurity concentration distributions

The specimen has a length of 1000 mm and a depth of 10 mm when the diameter is 30.7 mm. The molten zone is 100 mm long. Fig. 4(a) shows the distribution of C_O at the position in which the normalized distance is 0.9, when the initial impurity concentration in the specimen is 1 wt% and the heater traverse rate is 1 mm/min. By investigating the change in value of C_O through time, as shown in Fig. 4(a), we obtain the impurity concentration distribution. When we conduct the calculation with a three-dimensional model, impurity concentrations of all points in the semi-circular specimen can be obtained. By taking advantage of this, the impurity concentration distribution in the process direction is calculated based on the position in the plane perpendicular to the process direction. The impurity concentration distribution in the solid as a function of depth in the Z=0 mm mid-plane is shown in Fig. 4(b).

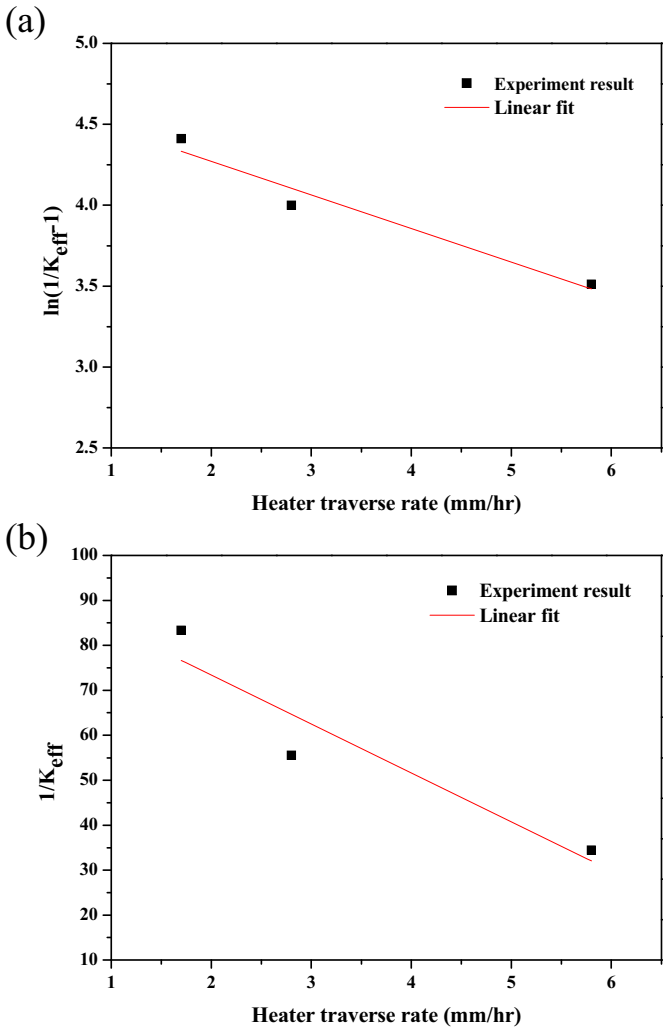

Fig. 3. Relation between (a) ln ($1/K_{eff}$-1) and the heater traverse rate and (b) $1/K_{eff}$ and the heater traverse rate.

The impurity concentration increases from the top of the specimen to the bottom, which contacts the boat. Fig. 4(c) shows the impurity profile in the liquid along the distance from the solid-liquid interface in the Z=0 mm mid-plane. One can see the diffusion boundary layer near the solid-liquid interface in this figure. The diffusion boundary layer becomes thicker as the depth increases, and as it becomes thicker, the impurities near the freezing interface become harder to wash away from the interface. This causes more impurities to accumulate near the interface at an increased depth. Therefore, the origin of the relation between the depth and the impurity concentration is the varying boundary layer thickness at the freezing interface.

The impurity concentration distribution was calculated in the process direction using the average values in the plane perpendicular to the process direction, for various heater traverse rates. When the heater traverse rate increases from 0.5 mm/min to 1 mm/min, the impurity concentration value increases throughout the entire specimen (Fig. 5(a)). As shown in Fig. 5(b), as the heater traverse rate increases, more impurities accumulate at the interface, even though the thickness of the diffusion boundary layer hardly varies. The thickness of the diffusion boundary layer is affected by the flow of the melt, which is affected by the temperature distribution originating from the external heater. In the three cases investigated, with traverse rates of 0.5 mm/min, 0.75 mm/min, and 1 mm/min, the thickness of the diffusion boundary layer does not change, because all three cases have the same temperature contribution. However, the rate of impurity accumulation

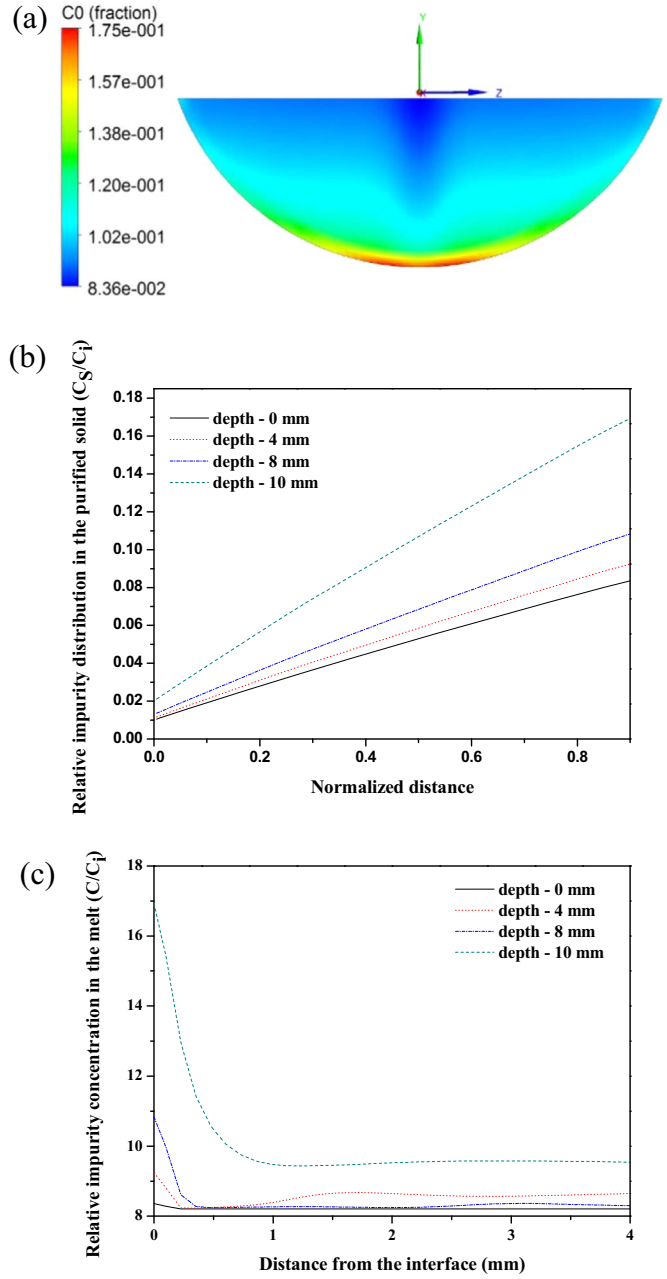

Fig. 4. Analysis of 3D results: (a) Impurity concentration profile in the melt at the freezing interface at the position in which the normalized distance (X) is 0.9. Impurity concentration distributions for different depths in the specimen (b) along the normalized distance (X) in the purified solid, and (c) along the distance from the freezing interface in the melt at the position at which the normalized distance of the freezing interface is 0.9.

at the interface increases as the heater traverse rate increases. Hence, the impurity concentration through the entire specimen increases as the heater traverse rate increases.

3.3. Decontamination factor

The decontamination factor is used as a criterion for the degree of impurity disposal, which is the purpose of this study. The decontamination factor is the ratio of the sum of the impurities in part of the initial specimen to that obtained after the process. We calculate the decontamination factors by using 90% of the specimen. Because normal freezing occurs at the end of the specimen, the impurities are enriched in that region. Hence, the region in which normal freezing occurs is removed after the process.

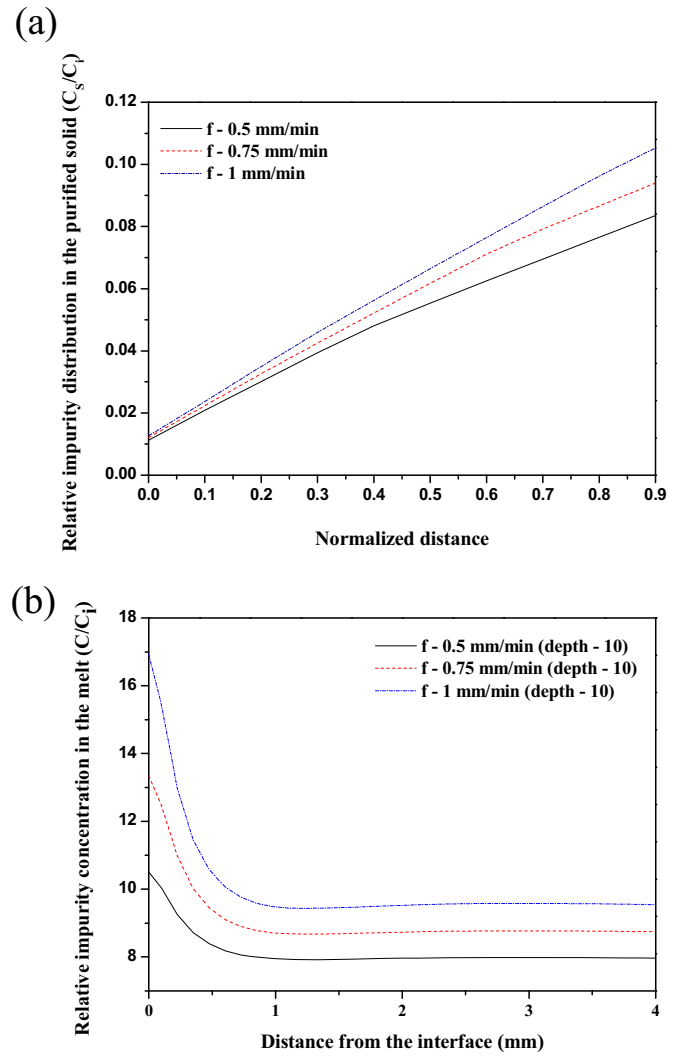

Fig. 5. Analysis of 3D results: Impurity concentration distributions for different heater traverse rates (a) along the normalized distance X in the purified solid (average values in the plane perpendicular to the process direction) and (b) along the distance from the freezing interface in the melt at the position in which the normalized distance of the freezing interface is 0.9 (values at depth=10 mm).

The 1D solutions are used to obtain the decontamination factors in terms of the number of passes. However, the 1D solution assumes that complete mixing takes place in the molten zone. In reality, however, complete mixing does not take place in the molten zone, as a boundary layer exists. To consider the degree of mixing in the molten zone, we apply the effective segregation coefficient obtained from this three-dimensional model to the 1D solutions. The effective segregation coefficient can be defined as [11]:

$$K_{eff} \equiv \frac{\overline{C}_S}{\overline{C}_L}, \tag{13}$$

where $\overline{C}_S$ denotes the average impurity concentration in the solid at the solid-liquid interface, and $\overline{C}_L$ is the average impurity concentration in the molten zone. In the present study, Eq. (13) is modified as:

$$K_{eff} = \frac{K_{eq}\overline{C}_O}{\overline{C}_L}, \tag{14}$$

where $\overline{C}_O$ denotes the average impurity concentration in the molten zone at the solid-liquid interface. Using Eq. (14), we calculate the effective segregation coefficients when 10%, 30%, 50%, 70%, and 90% of the process is completed (Fig. 6). The values of the average of the effective segregation coefficient and the standard deviation for each

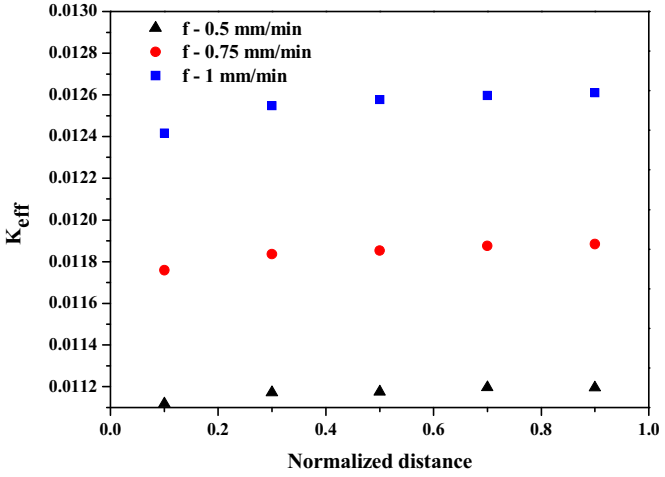

Fig. 6. Change of the K_{eff} through the process.

Table 1
The effective segregation values obtained from the 3-D simulation for different heater traverse rates.

Heater traverse rate (mm/min)	The average of K_{eff}	The standard deviation of K_{eff}
0.5	0.0112	2.8376e-5
0.75	0.0118	4.4862e-5
1	0.0126	6.9614e-5

heater traverse rate are listed in Table 1. The following values of the effective segregation coefficients: 0.0112, 0.0118, and 0.0126, are obtained at 0.5 mm/min, 0.75 mm/min, and 1 mm/min heater traverse rates, respectively. The deviation value of the effective segregation coefficient is 0.0025, 0.0038, and 0.0055 times the average value. Hence, we consider that the average value remains constant through the whole process, and can be used for 1D solutions.

With the 1D solutions and the effective segregation coefficient obtained from the three-dimensional transient model, we calculate the impurity distribution in the process direction. In the present study, the zone size for the analytical solutions is ten percent of the specimen, such as for the three-dimensional model. Fig. 7 shows the impurity concentration distributions as calculated by the 1D solutions with the following value of the effective segregation coefficient: 0.01255, and the

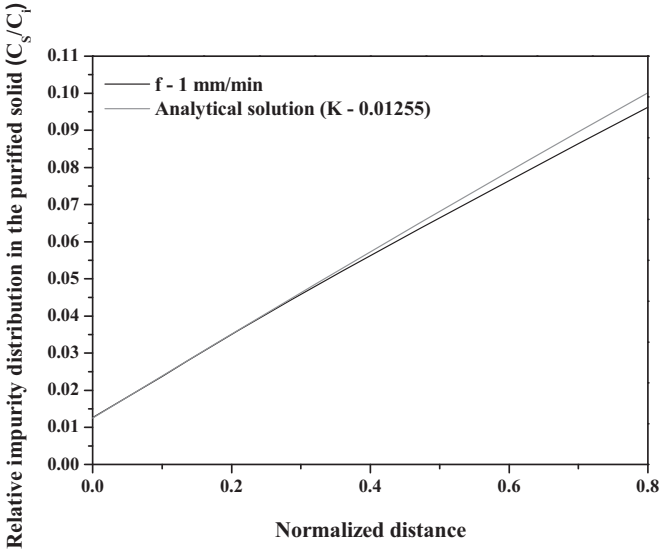

Fig. 7. Comparison of impurity concentration distribution between 3D simulations and 1D solutions with f=1 mm/min and K_{eff}=0.01255.

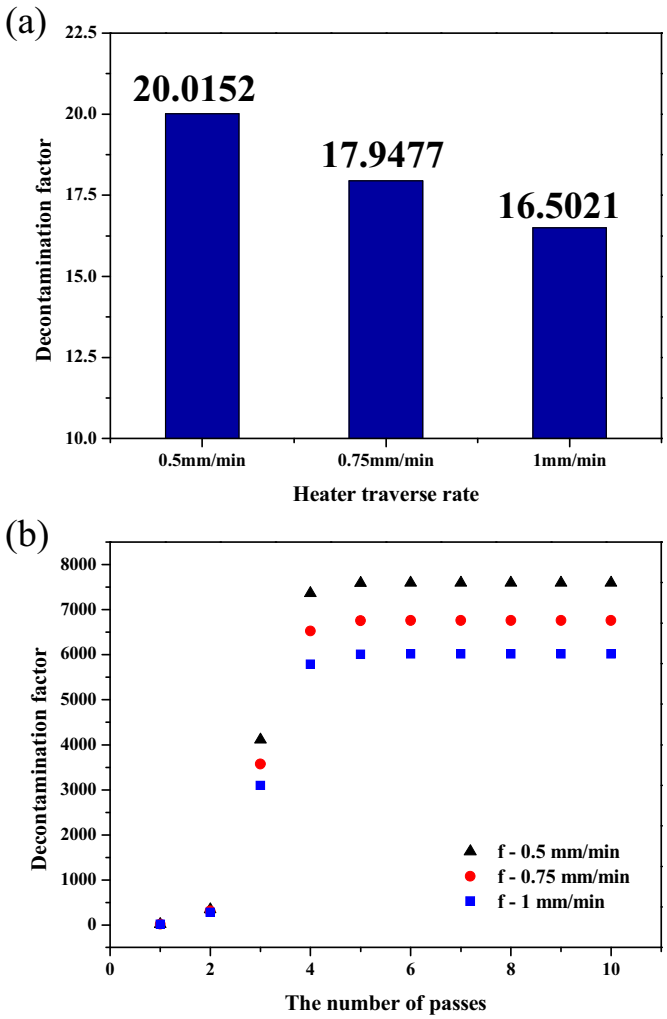

Fig. 8. Decontamination factors: (a) 3-d simulation results for 1 pass; (b) analytical solution results for multipass.

three-dimensional model with 1 mm/min heater traverse rate. The impurity concentration distributions calculated by both methods have similar tendencies that were also obtained the case of different heater traverse rates. Hence, the 1D solutions to which the effective segregation coefficient is applied may be used for calculating the decontamination factors for the multipass process.

Fig. 8(a) shows the decontamination factor as a function of the heater traverse rate. Values of 20.0152, 17.9477, and 16.5021 are obtained at 0.5 mm/min, 0.75 mm/min, and 1 mm/min heater traverse rate, respectively. For the decontamination factor, a larger value means that fewer impurities remain in the specimen after the process. As shown in Fig. 8(a), the lower the heater traverse rate is, the larger the decontamination factor is. This means that the ability of the zone refining process to dispose of impurities is improved as the heater traverse rate decreases. As the heater traverse rate decreases, the process proceeding rate also decreases, although the flow in the melt is barely affected. Hence, the case with the lower heater traverse rate allows more time for release of impurity accumulation at the freezing interface. Fig. 8(b) shows the decontamination factors in terms of the number of passes. The decontamination factor increases steeply for each heater traverse rate as the process is repeated. From the sixth pass, the decontamination factor remains constant. This means that the sum of the impurities in 90% of the specimen has little difference beyond that limit. Hence, each maximum purification is determined as a function of the heater traverse rate.

4. Conclusions

A three-dimensional transient model to simulate the zone refining process was developed. Fluid flow, mass transfer, and heat transfer in the melt are calculated with fixed interfaces. The non-vanishing wall velocity and subroutine make it possible to consider movement of the interfaces. The equilibrium segregation coefficient, derived from the effective segregation coefficient, is used in the calculation. The deeper the position is in the specimen, the higher the impurity concentration is in the process direction, which results from the difference in boundary layer thickness at different depths. As the heater traverse rate increases, more impurities are accumulated near the freezing interface. This brings about a higher impurity concentration in the process direction, whenever the heater traverse rate increases. From this model, the effective segregation coefficient is obtained as a function of the heater traverse rate. The impurity concentration distribution calculated by the 1D solution, along with the effective segregation coefficients, match well with those calculated by the three-dimensional model. The degree of impurity disposal, which is the purpose of this research, is measured by the decontamination factor. The decontamination factors were calculated in terms of the heater traverse rate when the equilibrium segregation coefficient was 0.01.

Acknowledgement

This work was supported by a National Research Foundation of Korea (NRF) grant funded by the Ministry of Science, ICT and Future Planning, Republic of Korea (MSIP). (NRF-2011-0031839).

References

[1] H. Lee, G.-I. Park, J.-W. Lee, K.-H. Kang, J.-M. Hur, J.-G. Kim, S. Paek, I.-T. Kim, I.-J. Cho, Current status of pyroprocessing development at KAERI, Sci. Technol. Nucl. Install. 2013 (2013).
[2] D. Lexa, I. Johnson, Occlusion and ion exchange in the molten (lithium chloride-potassium chloride-alkali metal chloride) salt+zeolite 4A system with alkali metal chlorides of sodium, rubidium, and cesium, Met. Mater. Trans. B 32 (2001) 429–435.
[3] A.N. Williams, S. Phongikaroon, M.F. Simpson, Zone Freezing Study for Pyrochemical Process Waste Minimization (MS Thesis), University of Idaho, Idaho Falls, ID, 2012.
[4] Y.-Z. Cho, G.-H. Park, H.-S. Lee, I.-T. Kim, D.-S. Han, Concentration of cesium and strontium elements involved in a LiCl waste salt by a melt crystallization process, Nucl. Technol. 171 (2010) 325–334.
[5] H.-S. Lee, G.-H. Oh, Y.-S. Lee, I.-T. Kim, E.-H. Kim, J.-H. Lee, Concentrations of CsCl and SrCl2 from a simulated LiCl salt waste generated by pyroprocessing by using Czochralski method, J. Nucl. Sci. Technol. 46 (2009) 392–397.
[6] J. Burton, R. Prim, W. Slichter, The distribution of solute in crystals grown from the melt Part I., Theor., J. Chem. Phys. 21 (1953) 1987–1991.
[7] J. Garandet, J. Favier, D. Camel, Solutal boundary layer concept and scaling analysis: two keys to segregation phenomena in melt crystal growth, J. Cryst. Growth 130 (1993) 113–122.
[8] A. Ostrogorsky, Effective convection coefficient for porous interface and solute segregation, J. Cryst. Growth 348 (2012) 97–105.
[9] A. Zaiour, M. Hage-Ali, J. Koebel, A. Bentz, P. Siffert, Equilibrium segregation coefficient and liquid diffusion coefficient of some impurities in tellurium, Appl. Phys. A 43 (1987) 219–222.
[10] J. Spim, M. Bernadou, A. Garcia, Numerical modeling and optimization of zone refining, J. Alloy. Compd. 298 (2000) 299–305.
[11] R.A. Brown, Modelling of directional solidification: from Scheil to detailed numerical simulation, J. Cryst. Growth 109 (1991) 50–65.